

Communication

A Nested SIW Cavity-Backing Antenna for Wi-Fi/ISM Band Applications

Divya Chaturvedi¹, Arvind Kumar², and Singaravelu Raghavan

Abstract—In this communication, a cavity-backed slot antenna is proposed using substrate-integrated waveguide (SIW) technology for Wi-Fi/Industrial, Scientific, and Medical Radio band applications. This antenna comprises two SIW cavities, a rectangular and circular with a circular ring slot on the top of each cavity for radiation. The circular cavity is designed such that it is nested inside the rectangular cavity, and each one is excited by separate feedlines (microstrip and coaxial probe). By properly optimizing the antenna dimensions, it produces two frequency bands at 5.2 and 5.8 GHz with a small frequency ratio of 1.12. Finally, the design is fabricated and the results are experimentally verified. The experimental results show that the proposed antenna exhibits a -10 dB impedance bandwidth of 6% (5.04–5.35 GHz) in the lower frequency band and 3.4% (5.73–5.92 GHz) in the higher frequency band with maintaining the input port isolation better than 28 dB. Due to the SIW cavity-backing structure, the antenna shows unidirectional radiation patterns at both resonant frequencies of 5.2 and 5.8 GHz with the gain of 6.97 and 6.2 dBi, respectively. Moreover, the antenna possesses the advantages of lightweight, planar configuration, and ease of fabrication.

Index Terms—Cavity-backed antenna, industrial, scientific, and medical radio (ISM) band, isolation, substrate-integrated waveguide (SIW).

I. INTRODUCTION

In recent years, with the proliferation of advanced wireless communication systems, the demand for low-profile dual-band antennas with high input port isolation has increased extensively [1], [2]. Simultaneous use of dual-frequency operation in transceivers requires two antennas, which confine their applications due to constraints of space and weight. The total area occupied by the antennas can be reduced considerably by consolidating different radiating elements in the shared-aperture configuration [3]. The antennas can share the same aperture by using different techniques such as stacking of elements, segmenting an aperture into subapertures, and inserting one resonator inside another resonator [4], [5]. However, the stacked configurations are complex and bulky in size, which restrict them to integrate with planar circuits and lead to large footprints. In the case of segmentation technique, an antenna aperture is divided into subapertures, and each one resonates at a specific frequency. By using this technique, the main challenge posed by these antennas is to have a high intrinsic isolation between the input ports. A defected ground structure is used to improve port isolation in [6]. However, such a structure leads to back radiations. A dual-band dual-polarized patch antenna is designed using a double-layered configuration in [7], where two-port feeding is provided using Wilkinson power divider while maintaining intrinsic input port isolation. However, the power divider-based feeding network increases the overall size

of the antenna assembly. Multilayered patch antennas [4], [8] based on electromagnetic bandgap and shared-aperture methodologies are employed to achieve high isolation and dual-band response.

In recent times, substrate-integrated waveguide (SIW)-based cavity-backed slot antennas have become a prevalent choice among the researchers due to their low footprints, cost-efficient fabrication, and integrability with the planar circuits [9]. SIW-based cavity-backed slot antennas for multifrequency operations with intrinsically isolated input ports are reported in [10]–[16]. All the above-mentioned designs provide the features of independent frequency tunability with maintaining printed circuit board (PCB) level circuitry. In addition, these antennas are found useful to avoid the decoupling/diplexing networks. Thus, the overall size of the RF front-end system is reduced. Due to their single-resonance radiation in each operating band, these antennas suffer from narrow operating bandwidth, typically $\leq 3\%$. Thus, enhancement in bandwidth is required to utilize these antennas for many practical applications. Shared-aperture antennas with improved operating bandwidth are reported in [17]–[19], where the high-frequency resonator is inserted into the lower frequency resonator. These antennas offer high gain with good radiation performance. In addition, these types of configurations eliminate the problem of limited bandwidth. As per the authors' knowledge, a limited work has been reported in the previous literature on shared-aperture type planar dual-band antennas.

In this communication, a novel nested SIW cavity-backed antenna is presented for Wi-Fi band (5.15–5.35 GHz) and Industrial, Scientific, and Medical Radio band (5.725–5.875 GHz) applications. It comprises two SIW cavities where a circular cavity is nested inside the rectangular cavity with individual radiating circular ring slots on the top metallic surface. Each cavity is excited individually with maintaining high isolation of 28 dB between input ports. Finally, the proposed design is fabricated using the standard PCB process. The experimental results show a good agreement with the simulated counterparts.

II. ANTENNA DESIGN AND PRINCIPLE OF OPERATION

The configuration of the proposed nested cavity-backed antenna is shown in Fig. 1. The proposed antenna is realized on a single-layered RT/Duroid substrate with dielectric constant of 2.2, loss tangent of 0.0009, and thickness of 1.57 mm. The rectangular SIW cavity (Cav1) is formed by connecting the top and bottom copper claddings with metallic vias, which form the lateral sides of the cavity. Similarly, a circular SIW cavity (Cav2) is formed by placing the metallic vias in a circular fashion. The dimensions of the rectangular SIW cavity ($L \times W$) are calculated from the waveguide equivalence model as described in [9]. The dimensions are estimated so as to support TE_{110} in the S-band (at 2.95 GHz) and TE_{120} mode in the C-band (at 4.65 GHz), respectively. The rectangular SIW cavity contains a circular ring slot of radius r_o (Slot1), width s , and it is excited by using an inset-based microstrip feedline. On the other hand, the circular SIW cavity is fed by a coaxial probe. A circular ring slot (Slot2) of radius r_i is introduced as a radiating element in the circular cavity. The slot radius has been calculated using the

Manuscript received May 7, 2018; revised January 15, 2019; accepted January 23, 2019. Date of publication January 31, 2019; date of current version April 5, 2019. This work was supported by the Ministry of Human Resource Development in the form of monthly Fellowship and Contingency NITT/RO/Ph.D. Cont. grant/2015. (Corresponding author: Divya Chaturvedi.)

The authors are with the Department of Electronics and Communication Engineering, National Institute of Technology Tiruchirappalli, Tiruchirappalli 620015, India (e-mail: divyanitt31@gmail.com; arvindchoudhary.eca@gmail.com; raghavan@nitt.edu).

Color versions of one or more of the figures in this communication are available online at <http://ieeexplore.ieee.org>.

Digital Object Identifier 10.1109/TAP.2019.2896670

0018-926X © 2019 IEEE. Personal use is permitted, but republication/redistribution requires IEEE permission.

See http://www.ieee.org/publications_standards/publications/rights/index.html for more information.

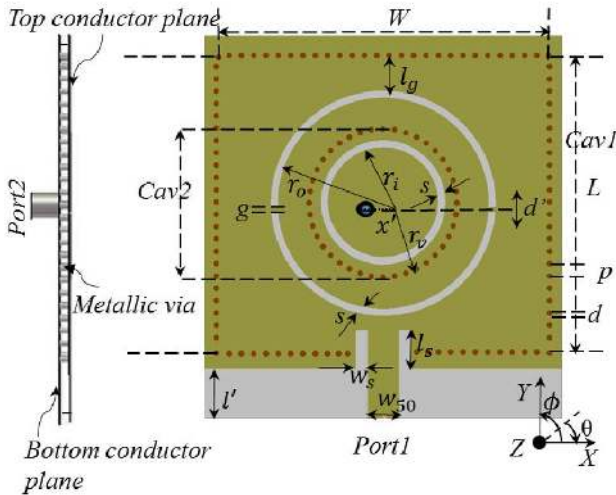


Fig. 1. Proposed nested SIW cavity-backed antenna configuration.

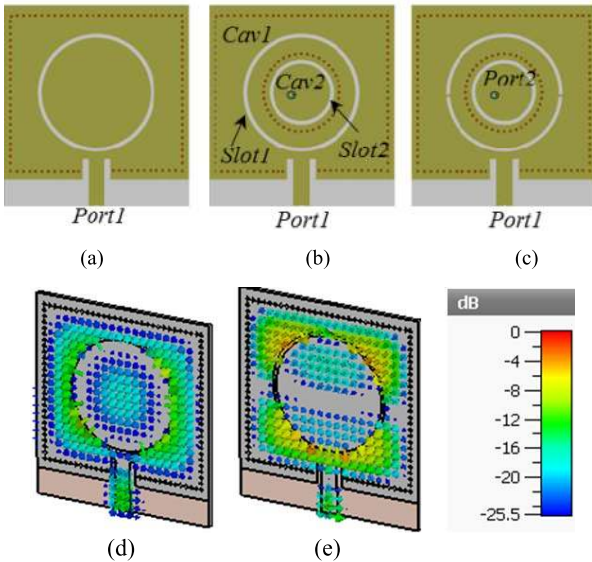


Fig. 2. Electric field vector at the top plane of the dielectric substrate in Prototype1. (a) Prototype1. (b) Prototype2. (c) Proposed antenna. (d) Modified TE₁₁₀ at 5.2 GHz. (e) Modified TE₁₂₀ mode at 5.65 GHz.

following equation suggested as in [20]:

$$f_r = \frac{K_{mn} c}{2\pi r_i \sqrt{\epsilon_{eff}}} \quad (1)$$

where c is the velocity of light in the free space, and ϵ_{eff} is the effective dielectric constant of the substrate. K_{mn} represents the corresponding root of Bessel's function and its value for the fundamental mode (TM₁₁) is 1.84. The design mechanism of the proposed antenna is illustrated in Fig. 2.

A. SIW Cavity-Backed Antenna With Single Cavity

A rectangular SIW cavity-backed antenna with a circular ring slot (Slot1) for radiation is shown in Fig. 2(a) and is labeled as Prototype1. The Slot1 is a nonresonant slot as its perimeter (C) is larger than the guide wavelength (for f_1 , $C = 2.6\lambda_g$, where λ_g is the guide wavelength at 5.2 GHz). The introduced slot divides the cavity into two parts (shortened outer aperture and parasitic inner circular aperture). Due to slot loading, the cavity modes (TE₁₁₀ and TE₁₂₀)

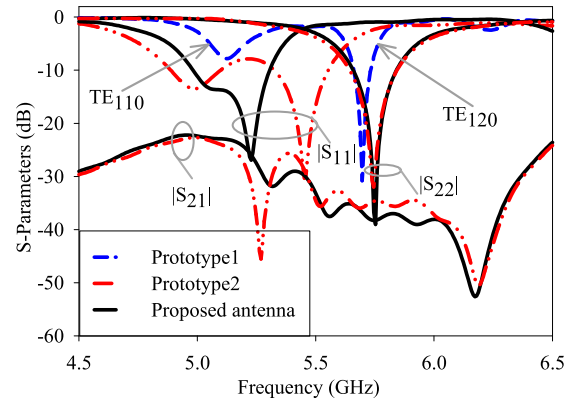


Fig. 3. S-parameters for different antenna configurations.

get perturbed and generate the modified modes TE₁₁₀ and TE₁₂₀ toward the higher frequencies at 5.2 and 5.65 GHz, respectively. Their electric field vector representations are shown in Fig. 2(d) and (e) and using commercially available software CST Microwave Studio (based on finite-integration time-domain algorithm). It can be observed in Fig. 2(d) that the original TE₁₁₀ cavity mode is influenced significantly by the slot and maximum field is concentrated in the outer shortened aperture of the slot loaded cavity, unlike original TE₁₁₀ cavity mode where maximum field concentrate at the center of the cavity. On the other hand, field distribution of the original TE₁₂₀ mode is slightly influenced by the slot. In the modified TE₁₂₀ mode, two half-wave variations can be observed along the slot with maximum field concentration at the shortened outer aperture. Thus, in both the above-mentioned cases, field intensity on the inner circular aperture appears weak and can be utilized to form another cavity resonator.

B. Proposed Nested SIW Cavity-Backed Antenna

A concentric circular SIW cavity resonator (Cav2) is nested inside the rectangular SIW cavity as shown in Fig. 2(b). This nested cavity configuration is labeled as Prototype2. A slot (Slot2) is introduced inside the Cav2 on the top cladding. To excite the slot loaded cavity, a separate coaxial-probe feed is used. The initial dimension of the slot is predicted by using (1). By properly optimizing the slot dimensions, the antenna produces a frequency band around 5.8 GHz. The location of the feed plays a critical role in exciting the cavity modes. It has been adjusted such that slot radiates in the fundamental TM₁₁ mode [23]. Due to the nested cavity configuration, an additional shunt inductance is generated which affects the resonance characteristics of the outer rectangular cavity. To compensate this, series capacitance is introduced by adding two conducting strips on Slot1, shown in Fig. 2(c). As a result, the modes around the frequencies of 5 and 5.5 GHz move in the close proximity and individual bandwidth get merged together in the desired frequency band. The individual bandwidth performance of the Prototype1, Prototype2, and the proposed antenna are illustrated in Fig. 3.

Due to the nested SIW cavity structure and orthogonal excitation of both the cavities, the proposed antenna exhibits adequate isolation level between the input ports. It can be clearly seen in Fig. 3 that the port isolation between Port1 and Port2 at lower and upper frequency bands is better than 28 and 32 dB, respectively. The radiation mechanism of the proposed design is explained with the help of the electric field distributions as shown in Fig. 4. As mentioned earlier, both the cavities are excited with the help of two individual feedlines. Fig. 4(a) and (b) shows the electric field distributions at

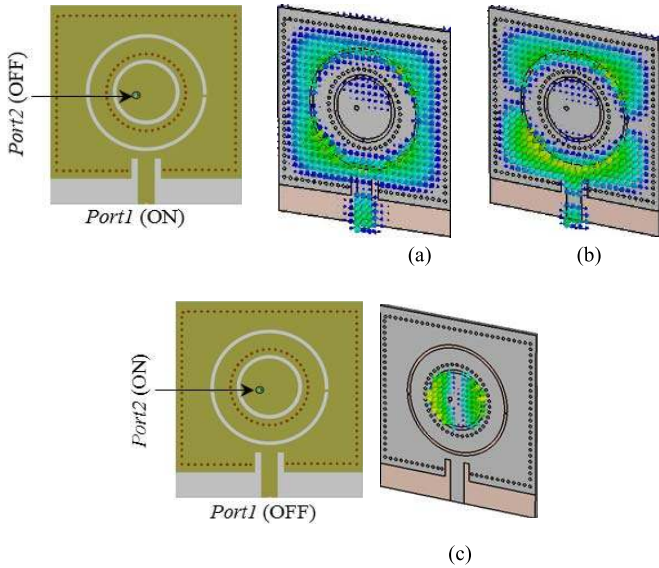


Fig. 4. Electric field vector at the top plane of dielectric substrate. (a) Modified TE₁₁₀ mode at 5 GHz (Port1: ON). (b) Modified TE₁₂₀ at 5.2 GHz (Port1: ON). (c) TM₁₁ mode at 5.8 GHz (Port2: ON).

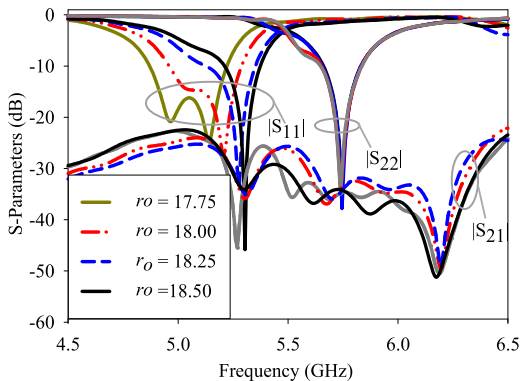


Fig. 5. Effect of Slot1 radius (r_o) on S-parameters.

two resonant frequencies of 5.0 and 5.2 GHz operating in the lower frequency band, and Fig. 4(c) shows the field distribution at the resonant frequency of 5.8 GHz operating in the upper frequency band.

In both of the above-mentioned cases, only a corresponding port is kept ON, while the other port is terminated (OFF) with 50 Ω matched port. It can be clearly observed that when one of the input ports is fed, the antenna radiates from the corresponding aperture while the other port remains unaffected. Thus, this configuration of radiating elements improves the isolation between the input ports.

III. PARAMETRIC ANALYSIS

To analyze the effects of key antenna parameters on the operating frequency bands, a parametric study is performed with the help of CST simulator. The effects of the radii of slots and the location of conducting strips on the resonances have been analyzed in Figs. 5–7. The input impedance and bandwidth at the lower frequency band predominantly depend on the radius (r_o) of Slot1. Variation of impedance matching and port isolation with a change in r_o is shown in Fig. 5. As the value of r_o increases, both the resonances in the lower frequency band shift to higher end. In the case of lower resonance, TE₁₁₀ mode acts as a nonresonant mode which completely depends upon the shortened aperture of Cav1. Consequently, frequency shifts to higher end with increasing r_o due to a reduction

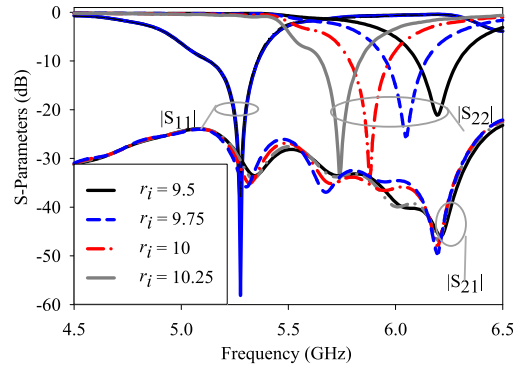


Fig. 6. Effect of Slot2 radius (r_i) on S-parameters.

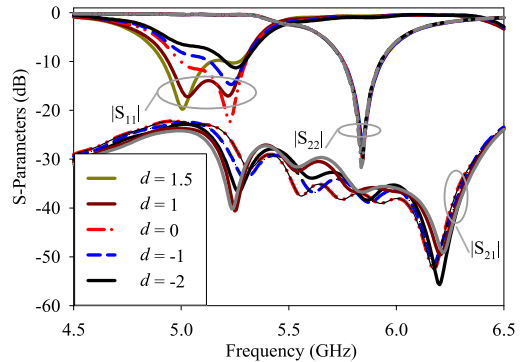


Fig. 7. Effect of strip locations on S-parameters.

in the effective aperture of the cavity. In the case of upper resonance, TE₁₂₀ mode acts as a resonant mode if $l_g > \lambda_g/4$, where λ_g is the guide wavelength at 5 GHz. On the other hand, if $l_g \leq \lambda_g/4$, the slot shows the opposite behavior than the conventional cavity-backed slot due to change in the boundary conditions [22]. The optimum value is chosen as $r_o = 18$ mm, which provides a frequency band around 5.2 GHz. Similarly, the effect on the higher frequency band with variation of the radius (r_i) of the Slot2 is shown in Fig. 6. As the value of r_i increases, the resonant frequency shifts toward the lower end, due to increment in the dimensions of the circular patch. The upper resonant frequency can be tuned within the frequency range of 5.75–6.25 GHz by varying r_i from 9.5 to 10.25 mm. As observed in Figs. 5 and 6, both the frequency bands can be tuned without affecting other resonant frequency with maintaining appropriate ports isolation. Thus, the design provides flexibility to tune the individual frequency band.

The effect of the location of conducting strips on the lower frequency band is shown in Fig. 7. When the strips shift upward along the y -axis, the corresponding resonant frequency band shift to the lower end and vice versa. This shift is found due to change in the lengths of two semicircular rings. The length of the lower semicircular ring increases when the strips are shifted in the upward direction. The lower semiring contributes more fringing field than the upper semiring. As a result, frequency band shifts toward the lower end with an increase in the length of the lower semiring. Furthermore, the effect of the position of coaxial feed on antenna performance is shown in Fig. 8. It can be seen that the location of feed significantly affects the isolation performance of the antenna. The isolation level in the multiports antenna can be improved by reducing the mutual coupling of the fields excited from the input ports [12]. Fig. 8 shows that the isolation level is poor when the feedlines of Cav1 and Cav2 are placed along the y -axis. This degradation in isolation level

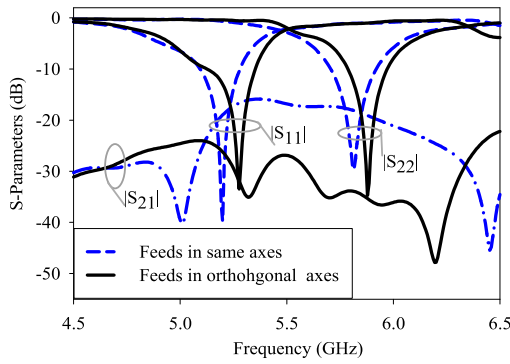
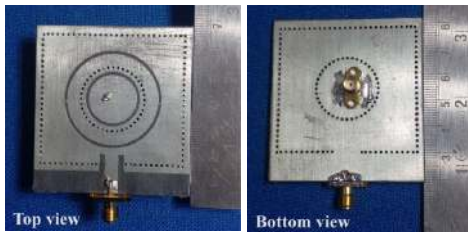


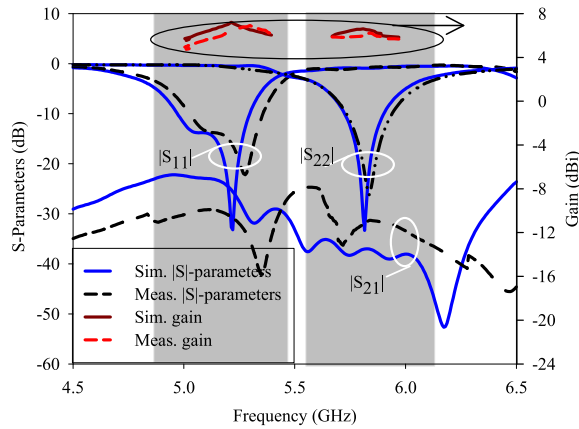
Fig. 8. Effect of feeds locations on S_{21} parameter.

TABLE I
DIMENSIONS (IN MILLIMETERS) FOR THE NESTED
CAVITY ANTENNA STRUCTURE

Parameter	value	Parameter	value
L	48	s	1
W	52	l'	7
r_o	18	d, p	1, 2
r_i	10.2	w_s	2.2
w_{50}	5	x'	2.5
g	0.5	l_s	6
l_g	4.5	d'	0



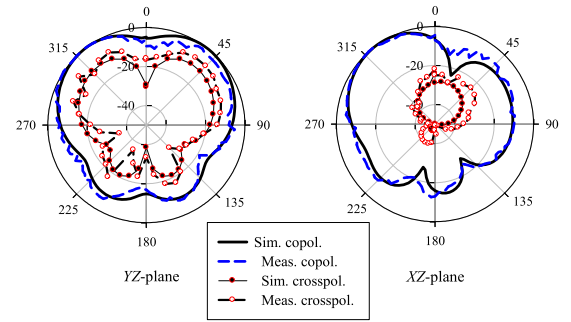
(a)



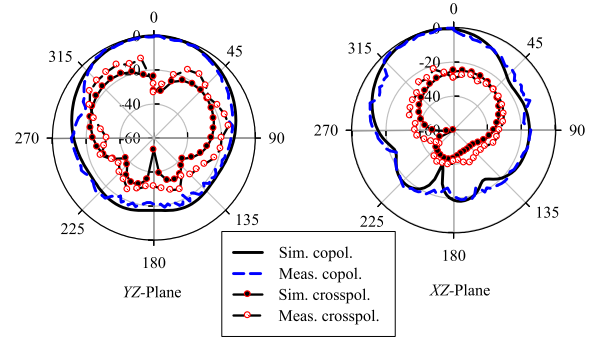
(b)

Fig. 9. (a) Photograph of the fabricated prototype. (b) S-parameters and gain plots.

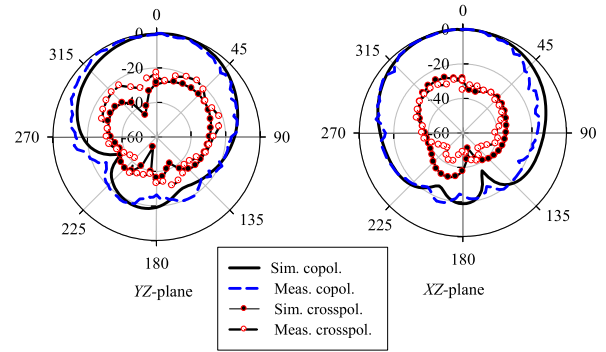
is obtained due to the presence of radiation nulls of both the cavity modes (TE_{120} mode of Cav1 and TM_{110} mode of Cav2) in the same plane. When both the cavities are excited orthogonally, the radiation nulls appear in orthogonal planes and the isolation level between ports is improved significantly. Moreover, the metallic wall of Cav2 plays a vital role in reducing mutual coupling. Finally, on the basis of simulation studies, the design guideline is summarized as follows.



(a)



(b)



(c)

Fig. 10. Simulated and measured radiation patterns at the yz -plane and xz -plane at (a) 5, (b) 5.2, and (c) 5.8 GHz.

- 1) Calculate the initial dimensions (L and W) of the rectangular cavity as suggested in [9].
- 2) Insert a circular ring slot of radius r_o as shown in Fig. 2(a) to excite the modified TE_{110} and TE_{120} modes for radiation. Tune the radius to excite both the modes in the desired frequency band (5–6 GHz).
- 3) Place a concentric nested circular SIW cavity with circular ring slot of radius r_i on its top metallic surface for higher frequency band resonance, shown in Fig. 2(b). Calculate the radius of the slot to get its dominant mode at the desired resonant frequency (i.e., at 5.8 GHz) with the help of (1).
- 4) Place two conducting strips on Slot1 to compensate the additional shunt inductance produced due to the inner circular cavity. Thus, with proper location of strips, two modes can be merged in the lower frequency band and so, bandwidth is enlarged.
- 5) Excite Slot2 in orthogonal axis to the Slot1 to minimize the mutual coupling effect.
- 6) Finally, the dimensions of the cavities and/or radius of the slots can be fine-tuned to adjust the frequency bands.

TABLE II
PERFORMANCE COMPARISON OF PROPOSED ANTENNA
WITH THE PREVIOUSLY REPORTED WORKS

Parameters	f_r (GHz)	Gain (dBi)	FBW (%)	Isolation (dB)	Size (λ_l) including feeding network
[10]	8.97	4.3	< 2	25	$2.6 \lambda_l \times 1.0 \lambda_l$
	11.2	4.2	< 2		
[11]	8.26	3.56	1.93	27.9	$1.3 \lambda_l \times 1.1 \lambda_l$
	10.46	5.24	2.68		
[12]	7.89	7.2	2.7	22.5	$1.3 \lambda_l \times 1.3 \lambda_l$
	9.44	7.2	2.0		
	9.87	7.2	1.8		
[13]	6.5	3.68	< 2	18	$1.0 \lambda_l \times 1.0 \lambda_l$
	7.6	4.76	< 2		
	9	4.5	< 2		
[15]	8.6	5.7	< 1	18	$1.3 \lambda_l \times 1.3 \lambda_l$
	9.8	5.9			
[16]	4.2	6.5	1.4	23	$1.2 \lambda_l \times 1.0 \lambda_l$
	5.2	4.2	2.5		
	5.8	5.8	2.4		
[22]	2.45	1.3	4	26	$0.83 \lambda_l \times 0.83 \lambda_l$
	5.5	4.4	18		
Proposed work	5.2	6.97	6.0	28	$1.5 \lambda_l \times 1.3 \lambda_l$
	5.8	6.2	3.4		

λ_l is the guiding wavelength at 5.2 GHz

IV. MEASUREMENT RESULTS

In order to verify the simulations, the proposed geometry is fabricated and tested. The optimized geometrical dimensions are shown in Table I. The photograph of the prototype is shown in Fig. 9(a).

All the measurements are performed with an Agilent Vector Network Analyzer E5071C. The measured S-parameters and gain performances of the proposed antenna are presented in Fig. 9(b) and agree well with the simulated counterparts.

The simulated results of -10 dB impedance bandwidth and peak gain values in the lower frequency band are 6.2% (4.97–5.29 GHz) and 7.1 dBi, respectively. The simulated results of -10 dB impedance bandwidth and peak gain value in upper frequency band are 3% (5.72–5.89 GHz) and 6.75 dBi, respectively. The measured impedance bandwidth of 6% (5.04–5.35 GHz) is obtained in the lower frequency band when Port1 is excited and Port2 is terminated by a matched load. Similarly, measured impedance bandwidth of 3.4% (5.72–5.92 GHz) is obtained when Port2 is excited and Port1 is terminated by a matched load. The measured port isolation level is also shown in Fig. 9(b) which is below -30 and -32 dB in lower and upper frequency bands, respectively. The measured gain values of the proposed antenna are 6.97 and 6.2 dBi at the frequency of 5.2 and 5.8 GHz, respectively. However, a slight discrepancy between the simulated and measured results is observed, which may be attributed to the fabrication imperfection and gain reduction due to dielectric losses.

The far-field radiation patterns at two principle cut planes of yz -plane ($\phi = 0^\circ$) and xz -plane ($\phi = 90^\circ$) of the proposed antenna for Port1 and Port2 are measured inside an anechoic chamber. The comparison of the simulated and measured radiation patterns at the frequencies of 5, 5.2, and 5.8 GHz is plotted in Fig. 10. It shows a dip in the broadside direction at 5 GHz as shown in Fig. 10(a), which is caused due to cancellation of the fields of the equal amplitude and same phase across the Slot1. On the other hand, the radiation patterns at the resonant frequencies of 5.2 and 5.8 GHz are unidirectional and oriented toward the broadside direction as shown in Fig. 10(b) and (c). The measured cross-polarization levels are 17, 32, and 29 dB in the yz -plane and 24.5, 24, and 27.5 dB in the xz -plane at the frequencies of 5, 5.2, and 5.8 GHz, respectively. In all cases, the measured front-to-back-ratio is better than 18 dB. The proposed antenna exhibits reduced backlobe radiation patterns due to the cavity-backed configuration. The overall size of the proposed antenna is $1.5\lambda_l \times 1.3\lambda_l \times 0.038\lambda_l$ (λ_l is the guide wavelength at a lower resonant frequency of 5.2 GHz). Moreover, the proposed design provides the combined advantages of conventional metallic cavity antenna (i.e., high gain and low backlobe radiation), and planar microstrip antennas (i.e., low profile, cost-efficient manufacturing using PCB, and ease of integration with planar microwave circuits).

To highlight the contribution of the proposed work, a performance comparison with the previously reported works is presented in Table II. It can be observed that the proposed antenna offers a better bandwidth performance compared to the works presented in [10]–[16] by using shared-aperture nested SIW cavity topology.

V. CONCLUSION

A nested SIW cavity-backed antenna is designed, fabricated, and validated. In the proposed configuration, a circular cavity is nested inside the rectangular cavity and circular ring slot is introduced on each cavity for the radiation. By properly exciting each cavity individually with the help of two distinct feeds, two frequency bands around the frequencies of 5.2 and 5.8 GHz have been produced with port isolation better than 28 dB. The use of the nested cavity approach optimally utilizes space and provides a flexibility in tuning the resonant frequencies independently. The measured results of the proposed design are in close proximity with the simulated results.

ACKNOWLEDGMENT

The authors would like to thank the editors and reviewers for their valuable comments and suggestions. They would also like to thank S. Purushothaman (Scientist ISRO Bangalore, India) for helping in the measurements at ISRO measurement laboratory.

REFERENCES

- [1] H. Lee, Y. Sung, C. T. M. Wu, and T. Itoh, "Dual-band and polarization-flexible cavity antenna based on substrate integrated waveguide," *IEEE Antennas Wireless Propag. Lett.*, vol. 15, pp. 488–491, 2016.
- [2] Z.-G. Liu and Y.-X. Guo, "Compact low-profile dual band metamaterial antenna for body centric communications," *IEEE Antennas Wireless Propag. Lett.*, vol. 14, pp. 863–866, Dec. 2014.
- [3] C. I. Coman, I. E. Lager, and L. P. Lighthart, "The design of shared aperture antennas consisting of differently sized elements," *IEEE Trans. Antennas Propag.*, vol. 54, no. 2, pp. 376–383, Feb. 2006.
- [4] S.-H. Hsu, Y.-J. Ren, and K. Chang, "A dual-polarized planar-array antenna for S-band and X-band airborne applications," *IEEE Antennas Propag. Mag.*, vol. 51, no. 4, pp. 70–78, Aug. 2009.
- [5] T. A. Axness, R. V. Coffman, B. A. Kopp, and K. W. O'Hare, "Shared aperture technology development," *Johns Hopkins APL Tech. Dig.*, vol. 17, no. 3, pp. 285–294, Jul. 1996.

- [6] Y. Chung, S.-S. Jeon, D. Ahn, J.-I. Choi, and T. Itoh, "High isolation dual-polarized patch antenna using integrated defected ground structure," *IEEE Microw. Wireless Compon. Lett.*, vol. 14, no. 1, pp. 4–6, Jan. 2004.
- [7] C.-Y.-D. Sim, C.-C. Chang, and J.-S. Row, "Dual-feed dual-polarized patch antenna with low cross polarization and high isolation," *IEEE Trans. Antennas Propag.*, vol. 57, no. 10, pp. 3321–3324, Oct. 2009.
- [8] L. Inclan-Sanchez, J. L. Vaquez-Roy, and E. Rajo-Iglesias, "High isolation proximity coupled multilayer patch antenna for dual-frequency operation," *IEEE Trans. Antennas Propag.*, vol. 56, no. 4, pp. 1180–1183, Apr. 2008.
- [9] F. Xu and K. Wu, "Guided-wave and leakage characteristics of substrate integrated waveguide," *IEEE Trans. Microw. Theory Techn.*, vol. 53, no. 1, pp. 66–73, Jan. 2005.
- [10] S. Mukherjee and A. Biswas, "Design of self-diplexing substrate integrated waveguide cavity-backed slot antenna," *IEEE Antennas Wireless Propag. Lett.*, vol. 15, pp. 1775–1778, 2016.
- [11] S. Nandi and A. Mohan, "An SIW cavity-backed self-diplexing antenna," *IEEE Antennas Wireless Propag. Lett.*, vol. 16, pp. 2708–2711, Aug. 2017.
- [12] K. Kumar and S. Dwari, "Substrate integrated waveguide cavity-backed self-triplexing slot antenna," *IEEE Antennas Wireless Propag. Lett.*, vol. 16, pp. 3249–3252, Dec. 2017.
- [13] A. Kumar and S. Raghavan, "A self-triplexing SIW cavity-backed slot antenna," *IEEE Antennas Wireless Propag. Lett.*, vol. 17, no. 5, pp. 772–775, May 2018.
- [14] D. Yang, F. Cao, and J. Pan, "A single-layer dual-frequency shared-aperture siw slot antenna array with a small frequency ratio," *IEEE Antennas Wireless Propag. Lett.*, vol. 17, no. 6, pp. 1048–1051, Jun. 2018. doi: [10.1109/LAWP.2018.2830760](https://doi.org/10.1109/LAWP.2018.2830760).
- [15] S. Nandi and A. Mohan, "SIW-based cavity-backed self-diplexing antenna with plus-shaped slot," *Microw. Opt. Technol. Lett.*, vol. 60, no. 4, pp. 827–834, Apr. 2018.
- [16] D. Chaturvedi, A. Kumar, and S. Raghavan, "An integrated SIW cavity-backed slot antenna-triplexer," *IEEE Antennas Wireless Propag. Lett.*, vol. 17, no. 8, pp. 1557–1560, Aug. 2018.
- [17] S.-S. Zhong, Z. Sun, L.-B. Kong, C. Gao, W. Wang, and M.-P. Jin, "Tri-band dual-polarization shared-aperture microstrip array for SAR applications," *IEEE Trans. Antennas Propag.*, vol. 60, no. 9, pp. 4157–4165, Sep. 2012.
- [18] R. L. Jordan, B. L. Huneycutt, and M. Werner, "The SIR-C/X-SAR synthetic aperture radar system," *IEEE Trans. Geosci. Remote Sens.*, vol. 3, no. 4, pp. 829–839, Jul. 1995.
- [19] D. M. Pozar and S. D. Targonski, "A shared-aperture dual-band dual-polarized microstrip array," *IEEE Trans. Antennas Propag.*, vol. 49, no. 2, pp. 150–157, Feb. 2001.
- [20] Q. Wu, H. Wang, C. Yu, and W. Hong, "Low-profile circularly polarized cavity-backed antennas using SIW techniques," *IEEE Trans. Antennas Propag.*, vol. 64, no. 7, pp. 2832–2839, Jul. 2016.
- [21] Z. C. Hao, X. Liu, X. Huo, and K. K. Fan, "Planar high-gain circularly polarized element antenna for array applications," *IEEE Trans. Antennas Propag.*, vol. 63, no. 5, pp. 1937–1948, May 2015.
- [22] Y.-C. Lu and Y.-C. Lin, "A mode-based design method for dual-band and self-diplexing antennas using double T-stubs loaded aperture," *IEEE Trans. Antennas Propag.*, vol. 60, no. 12, pp. 5596–5603, Dec. 2012.
- [23] D.-F. Guan, Z.-P. Qian, W.-Q. Cao, L.-Y. Ji, and Y.-S. Zhang, "Compact SIW annular ring slot antenna with multiband multimode characteristics," *IEEE Trans. Antennas Propag.*, vol. 63, no. 12, pp. 5918–5922, Dec. 2015.